# Ex Vivo Optical Coherence Tomography and Laser-induced Fluorescence Spectroscopy Imaging of Murine Gastrointestinal Tract

Lida P Hariri,[1,*] Alexandre R Tumlinson,[1] Norman H Wade,[2] David G Besselsen,[3,4] Urs Utzinger,[1] Eugene W Gerner,[5] and Jennifer K Barton[1,2]

Optical coherence tomography (OCT) and laser-induced fluorescence (LIF) spectroscopy each have clinical potential in identifying human gastrointestinal (GI) pathologies, yet their diagnostic capability in mouse models is unknown. In this study, we combined the 2 modalities to survey the GI tract of a variety of mouse strains and ages and to sample dysplasias and inflammatory bowel disease (IBD) of the intestines. Segments (length, 2.5 cm) of duodenum and lower colon and the entire esophagus were imaged ex-vivo with combined OCT and LIF. We evaluated 30 normal mice (A/J and 10- and 21-wk-old and retired breeder C57BL/6J) and 10 mice each of 2 strains modeling colon cancer and IBD (Apc$^{Min}$ and IL2-deficient mice, respectively). Histology was used to classify tissue regions as normal, Peyer patch, dysplasia, adenoma, or IBD. Features in corresponding OCT images were analyzed. Spectra from each category were averaged and compared via Student t tests. OCT provided structural information that led to identification of the imaging characteristics of healthy mouse GI. With histology as the 'gold standard,' we developed preliminary image criteria for early disease in the form of adenomas, dysplasias, and IBD. LIF characterized the endogenous fluorescence of mouse GI tract, with spectral features corresponding to collagen, NADH, and hemoglobin. In the IBD sample, LIF emission spectra displayed potentially diagnostic peaks at 635 and 670 nm, which we attributed to increased porphyrin production by bacteria associated with IBD. OCT and LIF appear to be useful and complementary modalities for ex vivo imaging of mouse GI tissues.

**Abbreviations:** GI, gastrointestinal; IBD, inflammatory bowel disease; IL, interleukin; LIF, laser-induced fluorescence spectroscopy; OCT, optical coherence tomography

Optical coherence tomography (OCT) is a nondestructive, high-resolution imaging modality that has been investigated for a vast array of applications, including imaging the anterior chamber of the eye[7] and intracoronary stenting.[3] Image contrast is produced from backscattering of near-infrared light at optical index mismatches, and resolutions of 5 to 20 µm typically are achieved.[12] OCT provides cross-sectional images with short penetration depths (1 to 2 mm) and can operate with either a water or air interface between the tissue and imaging probe.[12] OCT has been investigated as a method to image human gastrointestinal (GI) tissues and pathology.[12] In a study of in vitro human colon, OCT was capable of imaging the microstructure of the mucosal and submucosal layers.[9] In vivo, an OCT probe was used in conjunction with upper endoscopy, flexible sigmoidoscopy, and colonoscopy to evaluate OCT's abilities to image subsurface structures of human esophagus, stomach, duodenum, terminal ileum, colon, and rectum. High-resolution OCT images of the mucosa and submucosa were produced in all tested sites.[17] OCT also has been used to image colonic adenocarcinomas both ex vivo[20] and in vivo[14] and was able to differentiate normal and diseased tissue on a microstructural level.

Laser-induced fluorescence (LIF) spectroscopy measures the autofluorescence of biochemical components such as NADH, collagen, and porphyrin excited by ultraviolet to green wavelengths of light, providing biochemical information about a specimen. LIF has been used to evaluate a variety of tissue types, including normal and diseased human GI tissues, and has been found capable of distinguishing normal human colon from polyps and hyperplastic from adenomatous polyps both in vitro and in vivo.[15]

The complementary information provided by OCT and LIF (structural versus biochemical) merits the pairing of these 2 modalities, possibly providing a more sensitive and specific diagnostic technique than either unaccompanied modality. In a study using OCT and LIF to image neoplasms in the human cervix, false positives commonly produced by LIF from abnormally increased fluorescence due to inflammatory reactions were differentiated from cancer by the lack of structural changes visualized by OCT. Conversely, the atypical structure of scars appearing neoplastic in OCT was differentiated from cancer by the lack of abnormal LIF spectra. These 2 modalities combined produced fewer false-positive results than either modality alone.[10]

Mouse models of human pathologies can be used to enhance knowledge of pathologic processes and test therapeutic and chemopreventative compounds. Mouse models of colorectal cancer now available include the C57BL/6J-Apc$^{Min}$ strain, which exhibits an autosomally inherited predisposition to multiple intestinal neoplasia.[18] Mouse models of inflammatory bowel disease (IBD) also exist, such as the interleukin 2 (B6.129P2-Il2$^{tm1Hor}$, IL2)-deficient mouse. Mice deficient for IL2 have a 50% mortality rate by 9 wk of age. The remaining mice develop IBD that is clinically and histologically similar to ulcerative colitis and reportedly die

**Table 1.** Ex vivo normal and diseased groups

| | Strain | Age (wk) at image acquisition | No. of mice |
|---|---|---|---|
| Normal mice | C57BL/6J | 8–10 | 5 |
| | C57BL/6J | 20–21 | 5 |
| | C57BL/6J | 26–35 (retired breeders) | 5 |
| | A/J | 19 | 15 |
| Disease models | C57BL/6J-$Apc^{Min}$ (colonic adenomas) | 20–21 | 10 |
| | B6.129P2-$Il2tm1Ho$ (inflammatory bowel disease) | 8–10 | 10 |

Two of the normal mouse groups were used as respective age-matched controls for the disease mouse groups (21-wk-old C57BL/6J group for colorectal cancer group and 10-wk-old C57BL/6J group for IBD group). Ages for imaging of the diseased mice were chosen to correspond to life expectancy.

within 10 to 25 wk under conventional housing conditions.[16]

Although studies have shown that, individually, OCT and LIF have diagnostic promise in human GI pathology, it is unknown whether these imaging modalities can be applied to mouse models successfully, in light of differences in GI anatomy and the small size of structural features. Typically, analysis of disease in mouse models is performed by euthanizing animals at detected time points, followed by visual inspection and/or destructive tissue analysis. The motivation for the use of OCT and LIF lies in their noninvasive nature. These imaging modalities can be used for time-serial studies, for example, to track the growth of individual adenomas. We have shown in pilot studies that endoscopic OCT and LIF can be used to monitor the development of colorectal adenoma in the lower colon of $Apc^{Min}$ mice.[6,11] Ex vivo, their noninvasive characteristic makes them prime candidates as precursor modalities to destructive evaluation techniques, such as high-performance liquid chromatography. In vivo, OCT and LIF can be used endoscopically to image the colon or esophagus and can be used laproscopically to evaluate less-accessible regions of the GI tract, such as the small intestine.

There is no previously published systematic study of the mouse GI tract using OCT or LIF. We performed a pilot investigation to determine the appropriateness of 1) either modality for characterization of mouse colon, esophagus, and small intestine and 2) the synergy of OCT-LIF for this application. The main goal of this study was to determine the appearance of normal mouse GI tissue, by surveying different strains and ages with combined OCT-LIF. Secondly, we sampled disease from colorectal cancer and IBD mouse models to determine whether these pathologies were evident in one or both modalities. We developed preliminary image and spectral criteria for normal and diseased tissue that can be used to direct large-scale studies.

## Materials and Methods

**Animals.** Mice were purchased from Jackson Laboratories (Bar Harbor, ME), with the exception of the C57BL/6J-$Apc^{Min}$ mice, which were obtained from a colony maintained at the University of Arizona (Tucson, AZ).[4] Four groups of normal mice were included in this study: 1) 5 C57BL/6J mice at 10 wk, 2) 5 C57BL/6J mice at 21 wk, 3) 5 C57BL/6J retired breeders, and 4) 15 A/J mice. Two groups of diseased mice were included in this study: 1)10 $Apc^{Min}$ mice as models of colorectal cancer and 2) 10 IL2-deficient mice as models of IBD. Two of the normal mouse groups were used as respective age-matched controls for the disease mouse groups (21-wk-old C57BL/6J group for colorectal cancer and 10-wk-old C57BL/6J group for IBD). Both the IL2-deficient and $Apc^{Min}$ mouse models
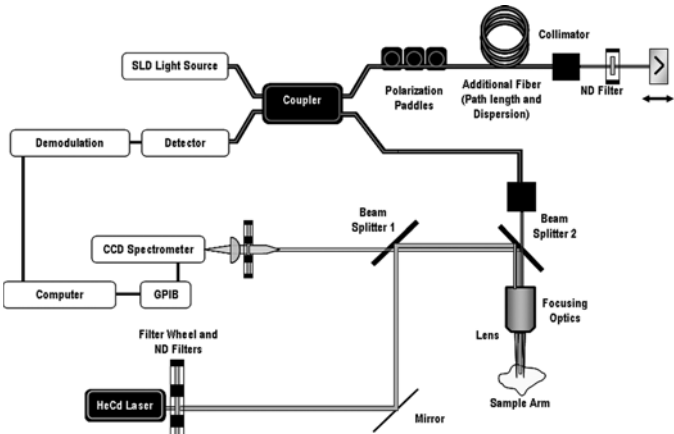


**Figure 1.** Schematic diagram of OCT-LIF system. The OCT subsystem source is a superluminescent diode (SLD) with a 1300 nm center wavelength. The LIF subsystem uses a He:Cd laser with excitation wavelengths of 325 and 442 nm. ND, neutral density.

spontaneously express disease. The strains, ages, and number of mice in the normal and diseased groups are summarized in Table 1. All mice were housed by University Animal Care (University of Arizona) in a pathogen-free environment in microisolator caging on a 12:12-h light:dark cycle with free access to water and standard laboratory chow. Protocols were approved by the University of Arizona Institutional Animal Care and Use Committee.

**Euthanasia, surgery, and tissue preparation.** Mice were euthanized with an overdose of 2.5% Avertin administered intraperitoneally. Sections of small intestine and colon 2.5 cm in length and the entire esophagus were removed from the mice. Small intestine samples were taken from the duodenum, 2.5 cm below the pyloric junction. Colon samples were taken just above the rectum. The entire esophagus was extracted for the esophageal samples by excising just below the larynx and above the gastroesophageal junction. All samples were flushed with saline to remove chyme and fecal matter when necessary. Each tissue sample was opened longitudinally and pinned with the luminal side up to a paraffin wax block. Tissue samples were bathed in 5% dextrose saline solution (Baxter, Deerfield, IL) until image acquisition. Prior to imaging, excess saline was removed with a cotton swab. The upper and lower bounds of the longitudinal OCT image and LIF data collection region were marked in the center line of each tissue sample with a permanent marking dye to aid in alignment of the OCT-LIF data with subsequent histologic sectioning. OCT images and LIF spectra were obtained from each tissue sample within 1 h of extraction.

**Table 2.** Data analyzed in the study

| Tissue | Mouse strain | No. of normal, Peyer patch (PP), and disease (inflammatory bowel disease [IBD] and adenoma–dysplasia [AD]) regions | | |
| | | OCT and histology | LIF (325 nm) | LIF (442 nm) |
|---|---|---|---|---|
| Colon | C57 10 wk | 5 normal | 5 normal | not applicable |
| | C57 21 wk | 4 normal | 4 normal | 4 normal |
| | C57 retired breeder | 5 normal, 1PP | 4 normal | 4 normal |
| | A/J | 12 normal, 4 PP | not applicable | not applicable |
| | Apc$^{Min}$ | 7 normal | 7 normal | 7 normal |
| | IL2-deficient | 7 normal, 1 IBD | 7 normal, 1 IBD | 5 normal, 1 IBD |
| Esophagus | C57 10 wk | 2 normal | 2 normal | 1 normal |
| | C57 21 wk | 5 normal | 5 normal | 5 normal |
| | C57 retired breeder | 1 normal | 1 normal | 1 normal |
| | A/J | 13 normal | not applicable | not applicable |
| | Apc$^{Min}$ | 6 normal | 6 normal | 4 normal |
| | IL2-deficient | 8 normal | 2 normal | 3 normal |
| Small intestine | C57 10 wk | 3 normal | 3 normal | 1 normal |
| | C57 21 wk | 5 normal | 5 normal | 5 normal |
| | C57 retired breeder | 5 normal | 4 normal | 5 normal |
| | A/J | 13 normal, 2 PP | not applicable | not applicable |
| | Apc$^{Min}$ | 5 normal, 1 PP, 6 AD | 5 normal, 1 PP, 6 AD | 5 normal, 6 AD |
| | IL2-deficient | 7 normal, 1 PP | 7 normal, 1 PP | 3 normal |

**OCT-LIF in-air system.** Figure 1 presents a diagram of the OCT-LIF system used in this study, which is similar to one previously described in detail.[2] The OCT subsystem used a superluminescent light source centered at 1300 nm with a 49 nm bandwidth, providing a 12 μm axial resolution in tissue. Light from the broadband source was split by a fiber-based Michelson interferometer into 2 paths: 1 path traveled to the sample arm where light was focused onto the tissue with a spot size (lateral resolution) of 14 μm. The other path traveled to the reference arm, which consisted of a galvo-mounted reference mirror. When the optical pathlengths of light backscattered from the sample and light reflected from the reference mirror were within the coherence length of the source, interference was detected. By moving the reference mirror, back-scattered light from various depths in the sample was collected. The tissue was translated laterally under the sample arm focusing lens in order to build up a 2-dimensional, cross-sectional image of the sample. Assuming an average tissue index of refraction of 1.4, the OCT imaging depth and lateral range were 1.42 mm and 9.0 mm, respectively. Each image contained 512 × 900 pixels and required approximately 64 s to acquire.

The LIF subsystem contained a helium-cadmium laser with excitation wavelengths at 325 and 442 nm; spectra were obtained separately at both wavelengths. Spectra were acquired continuously with approximately 4 spectra per mm acquired simultaneously with the OCT data. LIF is not depth-resolved; what was obtained from this subsystem was a series of emission spectra (fluorescence emission strength as a function of wavelength) for a series of lateral positions on the sample. Fluorescence spectra were corrected for background noise, autofluorescence, and spectral sensitivity of components. Oversampled spectral data were filtered to match the resolution of the system (10 nm).

**Histology.** Subsequent to image and spectra collection, tissue samples were adhered to Whatman filter paper to prevent tissue curling during fixation. After imaging, they were fixed in an alcohol-based fixative (Histochoice, Amresco, Solon, OH). Tissues were processed, embedded in paraffin, and sectioned saggitally. Dye marks applied prior to imaging were used to select histology sections corresponding to the location OCT and LIF data acquisition. Tissue sections then were stained with standard hematoxylin and eosin.

**Statistical analysis.** Histology was used as the 'gold standard' to classify regions of each OCT image and corresponding LIF spectra into normal, Peyer patch, adenoma, dysplasia, and inflammatory bowel disease. Features in OCT image regions corresponding to these classifications were noted. On the basis of histologic classification, LIF spectra were sorted into the 5 categories and normalized to 450 nm. Mean spectra were compared among C57BL/6J 10 wk, 21 wk, and retired breeder mice for each tissue sample type (colon, esophagus, and small intestine) by using unpaired Student $t$ tests. In addition, mean spectra for each disease and corresponding normal group pair were computed and analyzed using unpaired Student $t$ tests to determine any statistical differences. At each wavelength, a $P$ value was calculated and plotted. Fluorescence spectra correlating to adenoma and dysplasia were compared to determine any differences, but data for these groups then were grouped together for comparison with other classifications.

## Results

Table 2 indicates the analyzable data included in the study for each normal and diseased mouse group for the colon, esophagus, and small intestine. Table 2 also indicates the number of samples of normal, Peyer patch, IBD, and adenoma-dysplasia included in each normal and disease mouse group for each of the GI regions (colon, esophagus, and small intestine). Table 3 summarizes the data removed from the study. Of 150 OCT images and LIF spectral sets initially obtained, 46 were removed from analysis. OCT and LIF data was removed if tissue preparation error such as partially opened lumens or damage occurred (18% of data taken), technologic or instrument problems compromised the quality of the OCT image or LIF spectra such that the data were no longer

**Table 3.** Data removed from analysis

| Error | No. samples removed | % total error | % total data |
|---|---|---|---|
| Tissue preparation | 27 | 59.0 | 18.0 |
| OCT technologic | 1 | 2.0 | 0.6 |
| LIF technologic | 15 | 33.0 | 10.0 |
| Histologic artifact | 3 | 6.0 | 2.0 |
| Total | 46 | 100.0 | 30.6 |

OCT and LIF data was excluded if tissue preparation errors occurred, such as partially opened lumens and damage to prepared tissue, technologic problems compromised the quality of the OCT image or LIF spectra such that they could no longer be analyzed, or histologic artifacts were severe enough to prohibit analysis of the tissue.

analyzable (0.6% OCT, 10% LIF), or if histologic artifacts were severe enough that the sample was no longer analyzable (2%).

Example OCT images and histology of normal GI tract, Peyer patch, dysplasia, and IBD are presented. In Figures 2 A and B to 7 A and B, each figure illustrates an OCT image (Panel A) and its corresponding histology (Panel B). Figures 2 to 4 are images of normal C57BL/6J retired breeder colon, A/J esophagus, and A/J small intestine, respectively. The normal GI tract images are representative of the many images obtained; healthy tissues from all strains (normal and disease model) and all ages were similar in appearance. Figure 5 is an image of a Peyer patch in a normal section of an IL2-deficient small intestine. This image is representative of OCT images of Peyer patches seen in the small intestine and colon of other mouse strains and ages included in this study, although the patch size varied considerably. Seven examples of neoplasms were found in the small intestine of 6 Apc[Min] mice, including 2 dysplasias in 1 mouse and 1 adenoma each in 5 mice. Figure 6 presents an image of dysplasia in the Apc[Min] small intestine. One example of mild colitis was found in the upper colon of an IL2-deficient mouse and is presented in Figure 7. A summary of the OCT image features for all normal and diseased tissues is provided in Table 4.

The normalized 442-nm excitation LIF spectra for the IL2-deficient upper colon mild colitis and IL2-deficient normal colon are presented in Figure 8 over the 442 to 750 nm emission range. Error bars represent the standard error of the mean. Figure 9 displays a scatterplot of this data reduced to 635 and 670 nm emission wavelength fluorescence intensity. No other statistical differences were seen during comparisons of LIF emission spectra. A summary of the LIF spectra features for all normal and diseased tissues is provided in Table 4.

## Discussion

In this study, we were able to successfully survey and characterize the GI tract of 4 normal mouse groups—C57BL/6J at 10 wk, C57BL/6J at 21 wk, C57BL/6J retired breeders, and A/J mice—by using a combined OCT-LIF system. We also were able to image a colon cancer and IBD mouse model and identify early stages of colorectal cancer in the form of 7 adenomas and dysplasias as well as 1 case of early IBD in the form of mild colitis.

**OCT discussion.** The normal GI tract consists of multiple layers: the mucosa, submucosa, muscularis propria, and serosa.[8] The boundaries between these layers can be sites of optical mismatches visualized in OCT. Therefore, a thin line in an OCT image may correspond to a layer boundary, not an actual layer. However, if the layers are thick (>60 μm) and have differing backscattering properties, they could be differentiated according to grayscale (for example, one layer appears more hyperintense than another). Not all layers were sufficiently thick to be resolved in all images. Further, the submucosal and serosal layers in mice are quite thin (on the average of 6 to 60 μm) and usually could not be distinguished from the muscularis propria. The axial resolution of the OCT subsystem was 12 μm, and the pixel resolution of the photomicrographs was 1.3 μm pixels. Only features on the order of hundreds of microns will be discussed here. The OCT image and histologic features discussed for all normal and diseased tissues are summarized in Table 4.

Characteristically, the colonic mucosa is highly cellular, consisting of primarily enterocytes and goblet cells arranged in tubular crypts interlaced with regions of lamina propria. The muscularis propria of the colon is often thin, composed of 2 perpendicular layers of circularly and longitudinally arranged spindle-shaped myocytes with interposing enteric neuronal tissue.[8] Figure 2 A presents an OCT image of a normal retired breeder C57BL/6J mouse colon. The mucosal layer appears generally uniform in thickness, with moderate signal intensity and only mild signal attenuation over the depth of the layer. Crypt divisions, however, are too small to be resolved. Multiple hypointense pockets can be seen atop the mucosa, representing non-light-scattering fluid-filled pockets from the saline used to moisten the tissue during imaging. A thin, hyperintense region can be seen across the image just below the mucosa that is due to the index mismatch between the mucosal and submucosal layers, marking the boundary between these layers. The muscularis propria appears uniformly thin with a signal that is less intense than the mucosal signal. In this particular image, pancreatic tissue (labeled P) adhered to the abluminal side of the colon sample can be seen. The signal from the pancreas is moderate (between those of the mucosa and muscularis) and attenuates fairly rapidly with depth. In histology (Figure 2 B), the relative thicknesses of the mucosa and muscularis propria are in concordance with the thicknesses visualized in OCT. The presence of pancreas under the tissue sample corresponds well with the histology, in which the pancreatic tissue can also be seen.

Unlike the colonic mucosa, the esophageal mucosa is composed of primarily non-keratinized squamous epithelium. The muscularis propria consists of the same 2 layers of smooth muscle, but is often considerably thicker than the colonic muscularis.[8] An OCT image of a normal A/J mouse esophagus is presented in Figure 3 A. Note the relatively thin mucosa, presence of the submucosa, and thick muscularis propria. The mucosa displays a uniform thickness with moderate signal intensity and mild signal attenuation with depth. A bright backreflection can be seen at the surface of the mucosa across the majority of the image; we believe this signal to be due to large index mismatches between the surrounding air and either the mucosa or moistening saline. Below the mucosa is a hyperintense boundary separating the mucosal and submucosal layers. In the center of the image just below this boundary is a segment of submucosa, which is just thick enough to be visualized and is labeled. As expected, the muscularis propria is very thick, compromising the bulk of the image. The signal from the muscularis is hypointense compared with the mucosal layer, which is consistent with the findings seen in the colon. Interestingly, the boundary between the inner circular and outer longitudinal layers of the muscularis propria is partially visible. This feature can be expected, because a change in the muscle col-
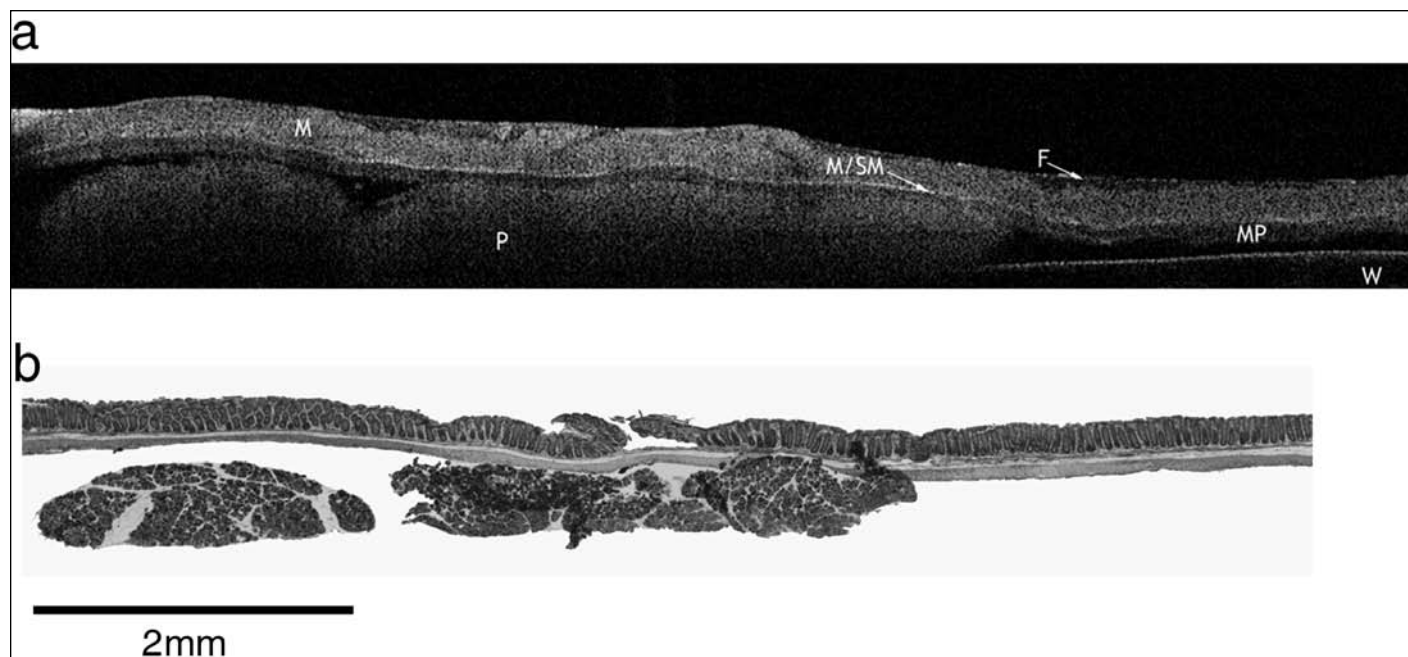
**Figure 2.** (A) OCT and (B) histology of colon from healthy C57BL/6J retired breeder mouse. The mucosa (M), mucosa-submucosa boundary (arrow labeled M/SM), and muscularis propria (MP) are labeled. The mucosa appears uniformly thick with moderate signal intensity and mild signal attenuation. The mucosal-submucosal boundary appears as a thin, hyperintense region below mucosa. The muscularis propria is thin with a hypointense signal relative to the mucosa. The muscularis propria-serosa boundary appears as a hyperintense region below the muscularis. The pancreas (P) is seen under the colon. The wax (W) under the colon to which the tissue was adhered during imaging is indicated, and the fluid film from the saline (arrow labeled F) is noted on the surface of the mucosa in OCT.
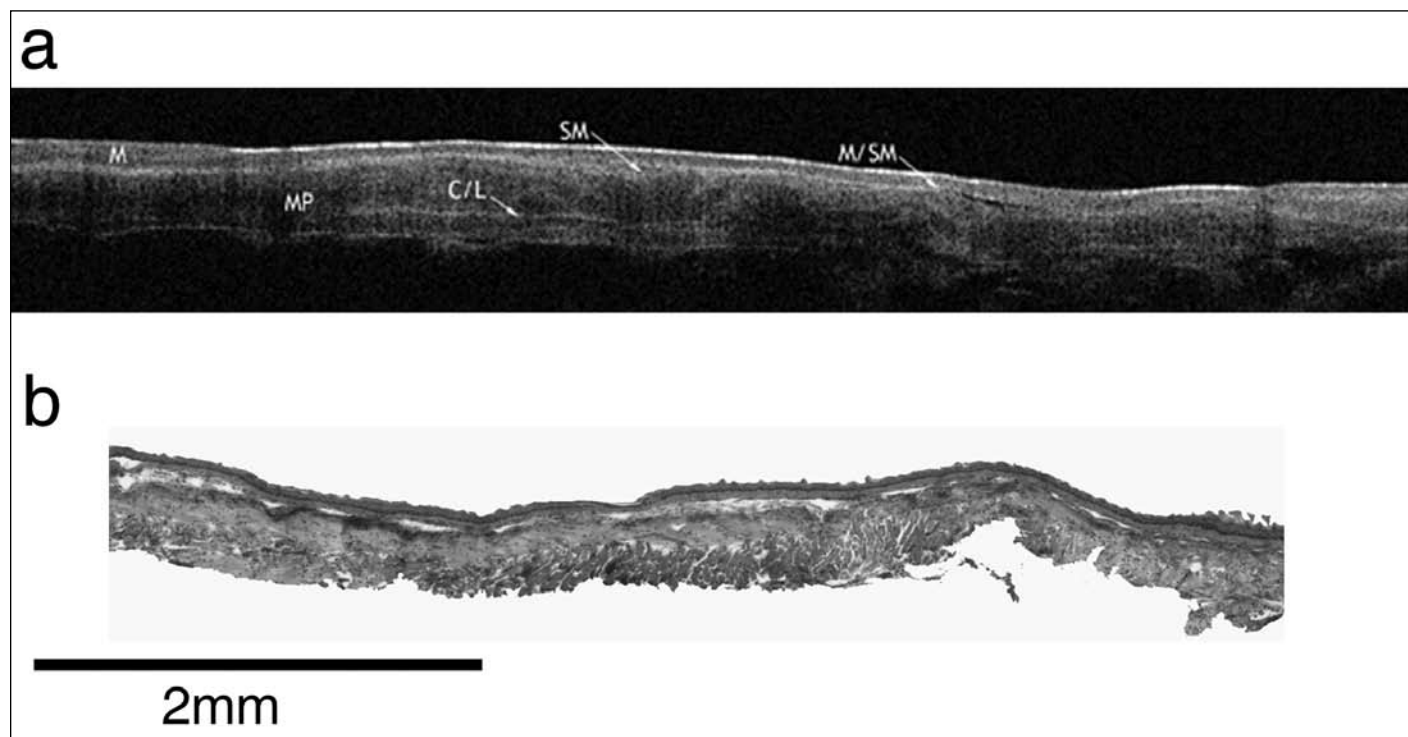


**Figure 3.** (A) OCT and (B) histology of healthy A/J mouse esophagus. The mucosa (M), mucosa-submucosa boundary (arrow labeled M/SM), submucosa (arrow labeled SM), submucosa-muscularis propria boundary (arrow labeled SM/MP), and muscularis propria (MP) are labeled. The mucosa appears thin with moderate signal intensity and mild signal attenuation. The mucosal-submucosal boundary appears as a thin, hyperintense region below the mucosa. The muscularis propria is thick with a hypointense signal relative to the mucosal signal. The muscularis propria-serosa boundary appears as a hyperintense region below the muscularis. Also interesting is the presence of the submucosa and the boundary between the inner circular and outer longitudinal muscle layers (arrow labeled C/L), which are not present in OCT images of other GI tissue.
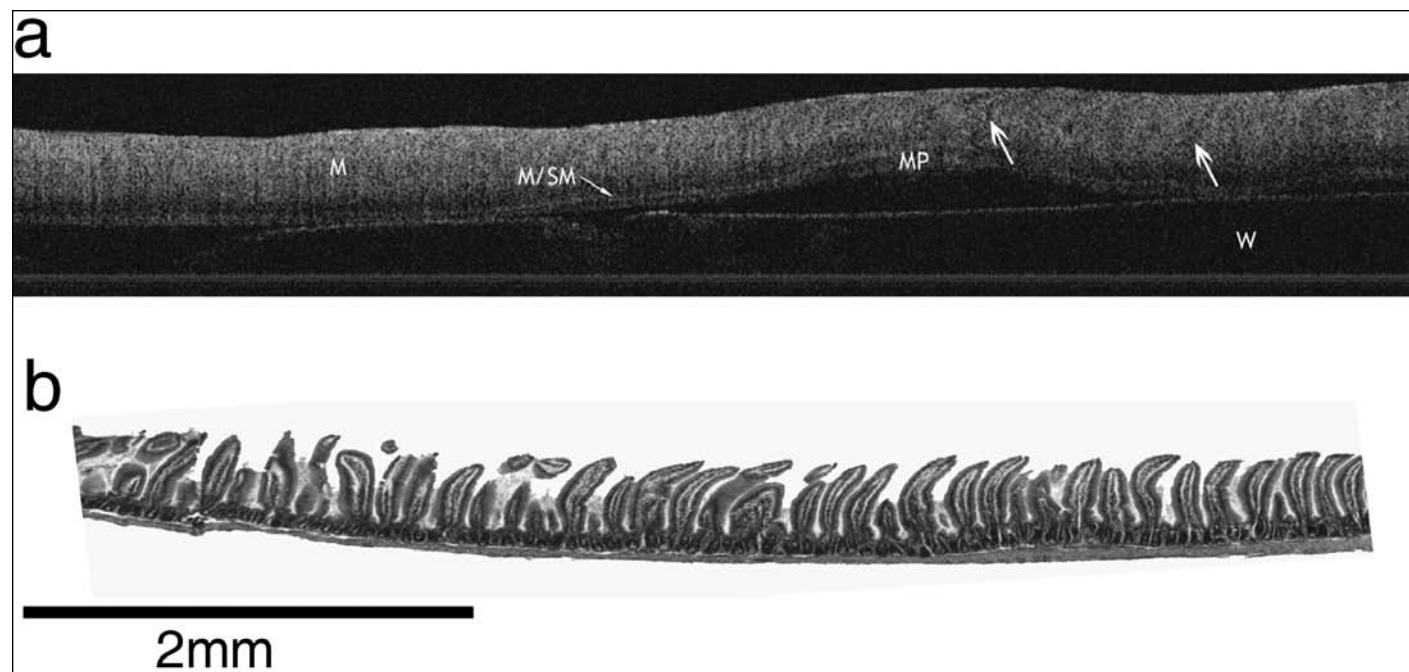
**Figure 4.** (A) OCT and (B) histology of healthy A/J mouse small intestine. The mucosa (M), mucosa-submucosa boundary (arrow labeled M/SM), and muscularis propria (MP) are labeled. The wax (W) under the colon to which the tissue was adhered during imaging is indicated. The mucosa appears thick with moderate signal intensity and mild to moderate signal attenuation. Faint vertical and diagonal black streaks (arrows) can be seen and most likely correspond to breaks between villi. The mucosal-submucosal boundary appears as a thin, hyperintense region below mucosa. The muscularis propria is thin with a less intense signal than the mucosa. The muscularis propria-serosa boundary appears as a hyperintense region below the muscularis.
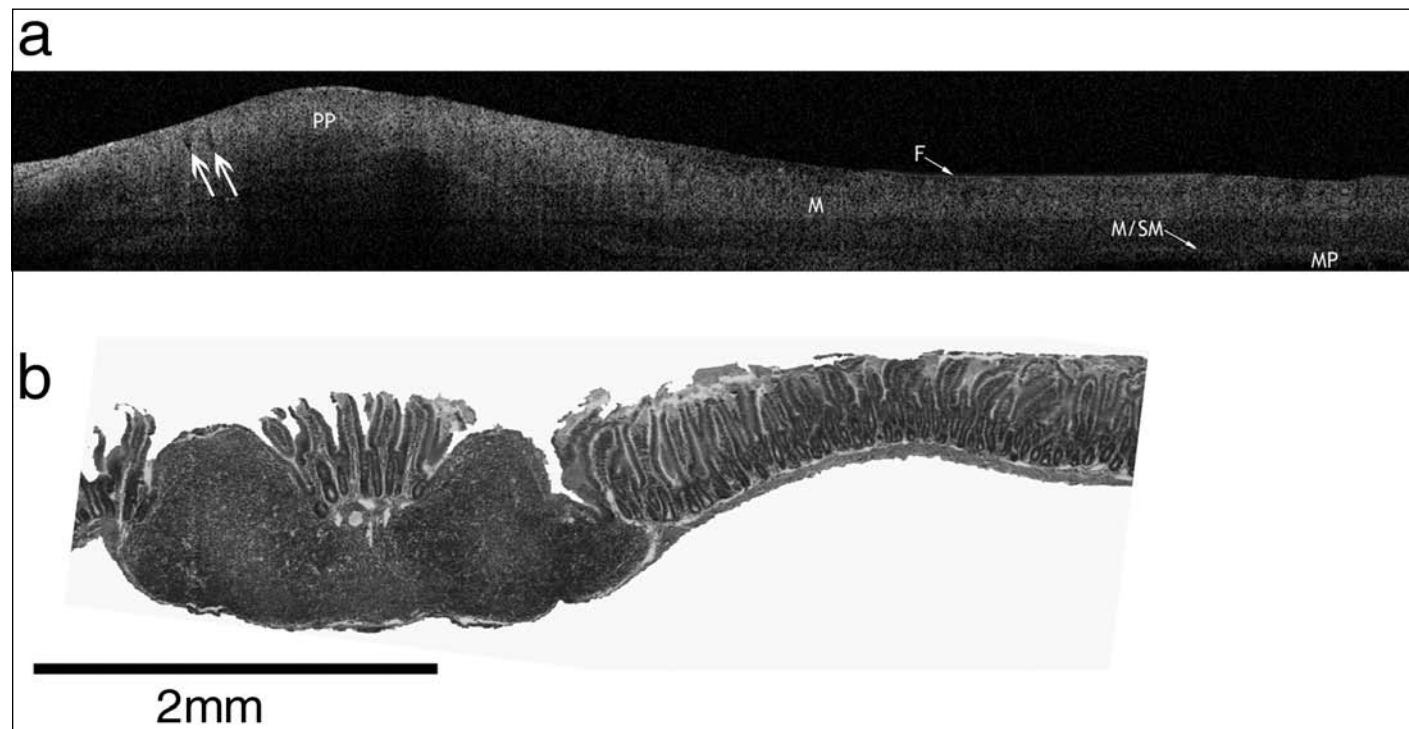


**Figure 5.** (A) OCT and (B) histology of a Peyer patch (PP) in an IL2-deficient mouse small intestine. The mucosa (M), mucosa-submucosa boundary (arrow labeled M/SM), and muscularis propria (MP) are labeled. The measured lengths and heights of the PP by OCT (2.10 and 1.25 mm, respectively) and histology (1.95 and 1.10 mm, respectively) were consistent. The height of the PP was greater than the OCT imaging depth, displacing the deeper tissue layers out of the image. The PP lacks the layered structure normally characteristic of the GI and exhibits moderate, homogeneous signal attenuation. On the borders of the PP, small vertical black lines (arrows) can be seen that are thought to correspond to spaces between villi. These villi also can be seen adjacent to the PP by histology. The fluid film from the saline (arrow labeled F) is noted on the surface of the mucosa in OCT.
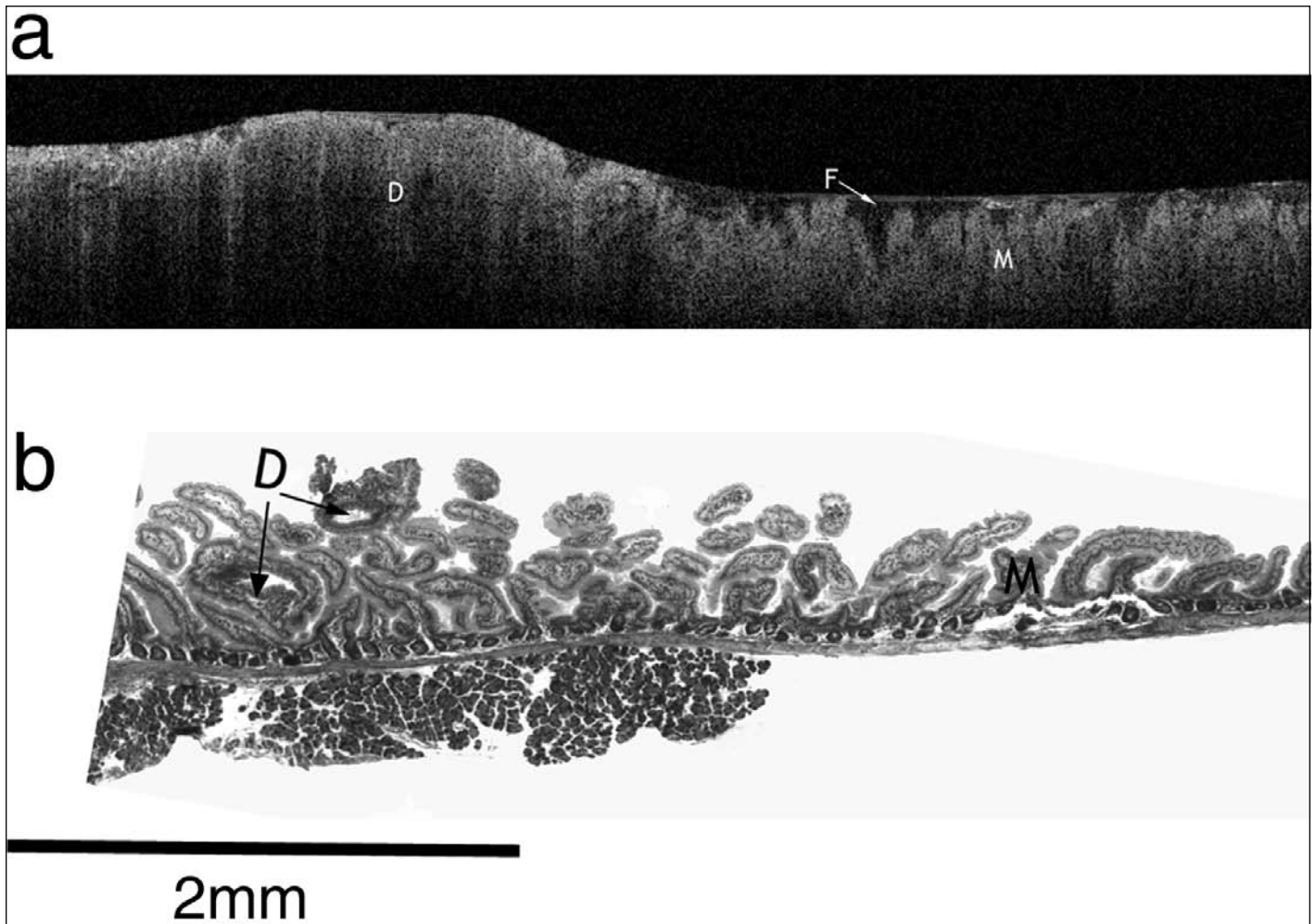
**Figure 6.** (A) OCT and (B) histology of dysplasia in an Apc$^{Min}$ mouse small intestine. The dysplasia (D) and adjacent normal mucosa (M) are labeled. The fluid film from the saline (arrow labeled F) is noted on the surface of the mucosa. (A) In the OCT image, the dysplastic region appears thickened, with an intense luminal signal and rapid, nonhomogeneous signal attenuation with depth into the mucosa when compared with healthy small intestinal mucosa. The mucosa adjacent to the dysplastic region appears to have elongated, far spaced villi. (B) The presence of elongated villi adjacent to the dysplasia is also visible by histology.

lagen orientation can create a specular reflection when the interface is normal to the OCT imaging beam. The relative thicknesses of the submucosa and muscularis propria in the histology appear to be in concordance with the thicknesses visualized in OCT. The mucosal layer appears to be thinner in the OCT image relative to the adjacent layers than in the corresponding histology. This appearance may be due to underlying muscle contractions that could occur in the ex vivo setting of OCT imaging, thereby causing the mucosa to appear thinner than it appears in histology.

The mucosa of the duodenal small intestine is relatively thick, characterized by elongated villi and short crypts composed of enterocytes and mucus secreting goblet cells.[8] The lamina propria extends into the core of each villus between the crypts and contains the lymphatic and vascular networks and the immune components for the mucosa. The muscularis propria again is composed of 2 layers of smooth muscle and has a thickness comparable to that of the colon. Figure 4 A presents an OCT image of a normal A/J small intestine. The mucosa is thick relative to the adjacent layers with moderate signal intensity and mild to moderate signal attenuation with depth. Faint, vertical and diagonal

black streaks can be seen within the texture of the mucosa, which may delineate villi; the resolution of the OCT system appears to be just great enough to differentiate some of these structures. A hyperintense boundary can be seen below the mucosa, delineating the mucosal-submucosal boundary. As was seen in the colon sample, the muscularis propria appears thin, and the signal is considerably hypointense relative to the mucosa. In the corresponding histology, the mucosa appears thick (Figure 4 B), and the muscularis propria thin, which is consistent with the relative thicknesses seen in the OCT image.

The intestinal tract contains its own local immune system, comprised of structures called Peyer patches, which are variably sized aggregations of lymphoid tissue.[8] Figure 5 A is an OCT image of a large Peyer patch (labeled PP) located in the mucosa of an IL2-deficient small intestine. The height of the Peyer patch was greater than the imaging depth, thus displacing the tissue layers deep to the Peyer patch out of the field of view. The Peyer patch lacks the layered structure apparent in the rest of the colon, and the OCT signal is moderately but homogeneously attenuated over the region. Atop the Peyer patch, faint vertical black lines can be
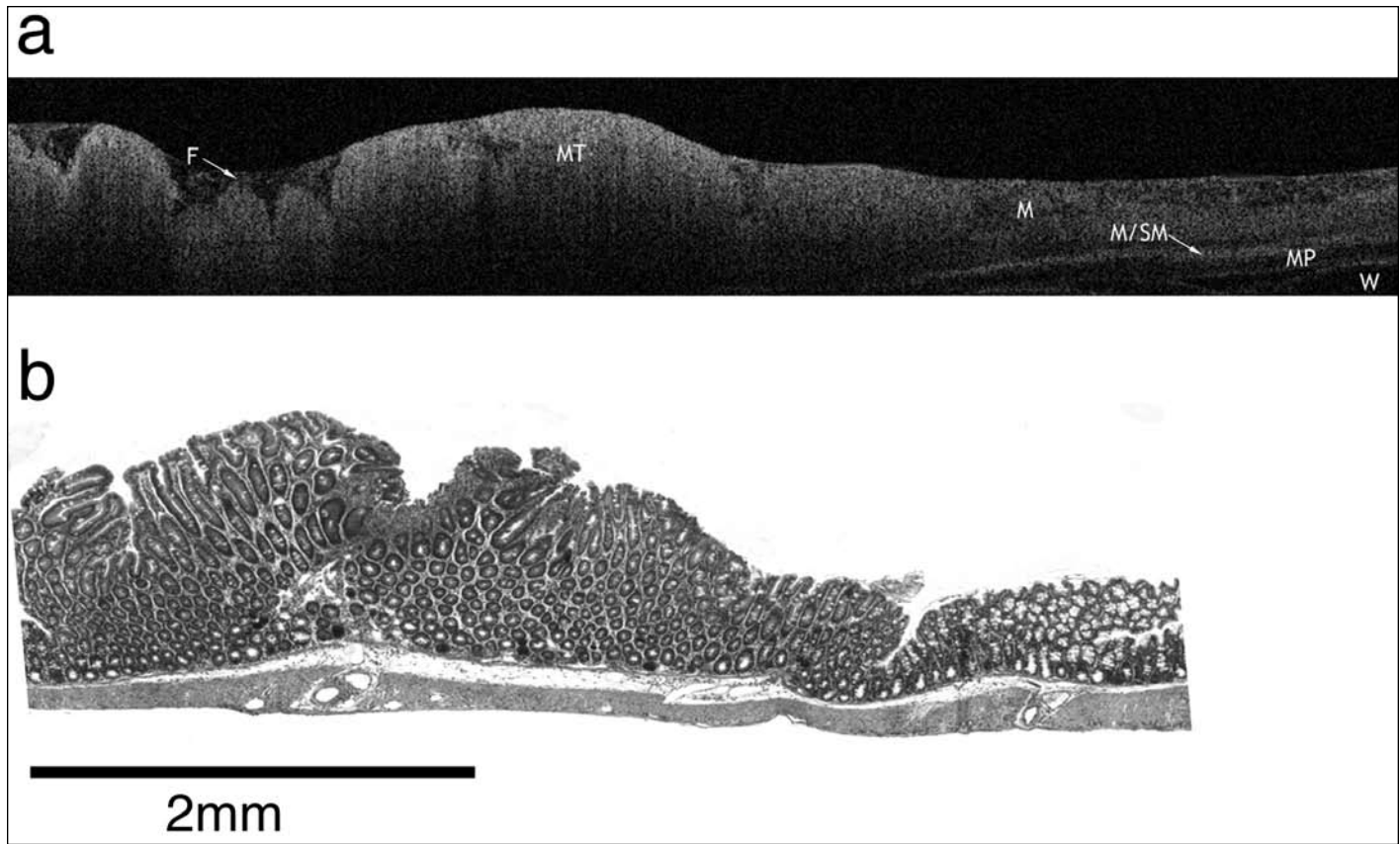
**Figure 7.** (A) OCT and (B) histology of mild colitis in an IL2-deficient mouse upper colon. The mucosal thickening (MT) associated with mild colitis is indicated. The adjacent normal mucosa (M), mucosa-submucosa boundary (arrow labeled M/SM), and muscularis propria (MP) are labeled. The mucosa of both the OCT and histology images is thickened to more than 1.4 mm in the inflamed region and has displaced the deeper layers out of the OCT imaging depth. The inflamed region displays intense luminal signal and mild, homogeneous signal attenuation with depth into the mucosa. On the right-hand side of the OCT image, the mucosa returns to a more normal thickness, and the muscularis propria can be seen. The wax (W) under the colon to which the tissue was adhered during imaging is indicated, and the fluid film from the saline (arrow labeled F) is noted on the surface of the mucosa in the OCT image.

seen; we think that these lines correspond to the spacing between villi located on the surface of the Peyer patch. The mucosa and muscularis propria of the small intestine adjacent to the Peyer patch appear very similar to those of the normal small intestine presented in Figure 4 A. Corresponding histology (Figure 5 B) reveals a large Peyer patch located in the intestinal mucosa with a number of villi seen atop the lymphoid tissue, all in concordance with the OCT image.

Dysplasias in the mucosal epithelium of the GI tract are believed to be precursor lesions to benign and malignant neoplasms that can surface in the small and large intestines. [13] An image of an Apc[Min] small intestine expressing 2 dysplasias (labeled D) in close proximity within the mucosa is presented in Figure 6 A. In the OCT image, the 2 dysplasias are undifferentiated from one another. The height of the mucosa containing the dysplasias was greater than the OCT imaging depth, thus displacing the layers deep to the region and the lower portion of the adjacent mucosa out of the field of view. The dysplastic region is characterized by mucosal thickening, marked nonhomogeneous attenuation of the OCT signal with depth, and a lack of the layered structure characteristic of normal colon. The more luminal regions of the mucosa appear to have a more intense OCT signal. The mucosal villi adjacent to the dysplastic region appear more elongated, slender, and diffuse than healthy intestinal villi. Elongation enables visualiza-

tion of the villi in this OCT image; normally they are not as easily discernable in images of healthy small intestine (Figure 4 A). In the corresponding histology (Figure 6 B), both dysplasias are visible, spaced in close proximity, and display enlarged, elongated villi with characteristic dysplastic changes in the affected cells. Elongated villi can also be seen in the mucosa adjacent to the dysplastic region. In the OCT image, the dysplastic region appears to have a longer lateral span than is seen in histology. The OCT and histology sections may have been taken at slightly different lateral locations within the tissue, such that the OCT image was obtained from the center of the dysplastic region and the histologic section was taken from the periphery of the region.

The IL2-deficient mice express disease resembling ulcerative colitis in humans, thus disease is restricted to mucosal and submucosal involvement. In inflamed regions, mucosal changes include marked thickening, ulceration, crypt branching, lymphocyte infiltration, and loss of goblet cells.[16] IBD in the proximal colon of an IL2-deficient mouse is presented in Figure 7 A. The inflamed mucosa (labeled MT) in the OCT image is markedly thickened to greater than the OCT imaging depth and has subsequently displaced the deeper layers out of the image. The more luminal regions of the mucosa appear to have an intense OCT signal, which is then mildly and homogeneously attenuated with depth. The characteristic layering of the colonic mucosa seen in

**Table 4.** Summary of tissue features

| | OCT | Histology | LIF emission |
|---|---|---|---|
| Normal colon | **M:** Moderate thickness, mild signal attenuation, bright M-SM boundary. **MP:** Thin, hypointense, bright MP-S boundary. | **M:** Simple columnar epithelium in tubular crypts with intervening lamina propria. **MP:** Thin layer of C-L smooth muscle. | Peaks from collagen at 380 nm, NADH at 450 nm, hemoglobin absorption at 420 nm. |
| Normal esophagus | **M:** Thin, mild signal attenuation, bright M-SM boundary, SM occasionally visible. **MP:** Thick, hypointense, bright MP-S boundary, C-L boundary occasionally visible. | **M:** Thin layer of nonkeratinized squamous epithelium. **MP:** Thick layer of C-L smooth muscle | Peaks from collagen at 380 nm, NADH at 450 nm, hemoglobin absorption at 420 nm. |
| Normal small intestine | **M:** Thick, mild to moderate signal attenuation, faint vertical or diagonal dark streaks occasionally visible, bright M-SM boundary. **MP:** Thin, hypointense, bright MP-S boundary. | **M:** Thick layer of simple columnar epithelium in villi with intervening lamina propria. **MP:** Thin layer of C-L smooth muscle. | Peaks from collagen at 380 nm, NADH at 450 nm, hemoglobin absorption at 420 nm. |
| Peyer's patch | Variations in size, moderate homogeneous signal attenuation, faint dark lines atop some PP may delineate villi on surface, lacks layered structure. MP often displaced out of field of view. Adjacent tissues appear normal. | Variably sized aggregations of lymphoid tissue present in the GI wall. May or may not have overlying mucosal tissue. | Peaks from collagen at 380 nm, NADH at 450 nm, hemoglobin absorption at 420 nm. |
| Dysplasia and adenoma | **M:** Thickening, strong nonhomogeneous signal attenuation, bright surface signal, lacks layered structure. **MP:** Often displaced out of field of view. Adjacent mucosa often displays elongated villi. | **M:** Enlarged, elongated villi with characteristic dysplastic changes to the enterocytes. Believed to be precursor lesions to benign and malignant neoplasms that can surface in the small and large intestines. | Peaks from collagen at 380 nm, NADH at 450 nm, hemoglobin absorption at 420 nm. No statistical difference from normal tissue. |
| Inflammatory bowel disease | **M:** Thickening, mild homogeneous signal attenuation, bright surface signal, lacks layered structure. **MP:** Often displaced out of field of view. | **M:** Considerable thickening, ulceration, crypt branching, lymphocyte infiltration, loss of goblet cells | Peaks from collagen at 380 nm, NADH at 450 nm, hemoglobin absorption at 420 nm. Peaks at 635 and 670 nm correspond to bacterial porphyrin production. |

C, circular; L, longitudinal; M, mucosa; MP, muscularis propria; PP, Peyer patch; SM, submucosa; S, serosa.

the control images (Figure 2 A) is not apparent in the inflamed region of the IBD mucosa. On the right side of the OCT image, the mucosa return to a more normal thickness and texture, and the muscularis propria can be visualized. In the corresponding histology (Figure 7 B), the inflamed region is markedly thickened with a higher density of villi. The adjacent mucosa and muscularis propria appear normal.

Visually, the IBD (Figure 7 B), dysplasia (D, Figure 6 A) and Peyer patch (PP, Figure 5 A) OCT images share similar characteristics and could potentially be difficult to differentiate. However, the signal attenuation seen in the dysplasia is nonhomogeneous compared with the more homogeneous attenuations visualized in the IBD and Peyer patch OCT images, therefore it likely is possible to distinguish dysplasia from both IBD and Peyer patch. The IBD OCT image has a slightly milder attenuation than does the Peyer patch OCT image; however, the slight differences may make it difficult to distinguish these categories using only OCT images (Table 4). An automated image analysis, such as texture analysis,[5] may be able to distinguish IBD and Peyer patches more readily. Due to the small number of lesions for each of these categories, a larger scale study must be conducted to confirm the applicability of these features for differentiating IBD, PP, and dysplasia.

**LIF discussion.** LIF previously has been evaluated as a mechanism for differentiating diseased and healthy regions in the GI tract. Fluorescence emission spectra from healthy human GI tract exhibit autofluorescence emission peaks from collagen and NADH at 380 and 450 nm, respectively, with a hemoglobin absorption dip at 420 nm. Emission spectra from human adenomatous colonic tissue have been characterized by a decrease in collagen autofluorescence and an increase in hemoglobin absorption.[15] The normal flora of the GI also has been characterized, with emission peaks at 635 and 670 nm, corresponding to their protoporphyrin production.[19]

The LIF spectral features discussed for all normal and diseased tissues are summarized in Table 4. All tissue samples of various strains and ages displayed characteristic fluorescence emission peaks at 380 nm from collagen, 450 nm from NADH, and a 420-nm hemoglobin absorption dip (Table 4). Student $t$ test comparisons of fluorescence emission spectra between diseased and respective normal mouse groups revealed no significant differences between any of the classifications (normal, dysplasia or adenoma, Peyer patch) within a group and tissue type (colon, esophagus, small intestine), with the exception of the single case of IBD in an IL2-deficient mouse.

The inflamed upper colon of this mouse exhibited peaks at 635 and 670 nm after excitation with the 442-nm wavelength (Figure 8); these results are in agreement with data in the literature describing the characterization of bacteria in the GI tract.[19] We believe that these peaks originate from the porphyrin produced by the bacteria in the inflamed colon (Table 4). The minimal overlap
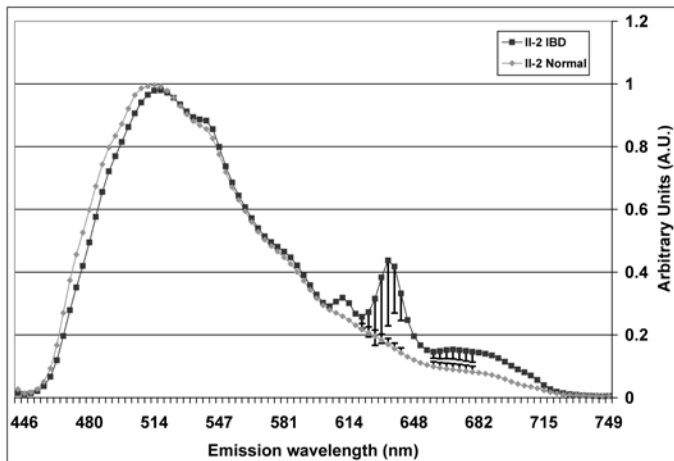
**Figure 8.** Normalized mean emission spectra from IL2-deficient upper colon with mild colitis and healthy IL2-deficient colon at an excitation wavelength of 442 nm. Error bars represent the standard error of the mean. Visible in all spectra are emission peaks from collagen at 380 nm, NADH at 450 nm, and a hemoglobin absorption dip at 420 nm. There are peaks present in the IL2-deficient mild colitis curve at emission wavelengths 635 and 670 nm; we attribute these peaks to porphyrin production by the infiltrating bacteria associated with the disease.



**Figure 9.** Scatterplot of emission wavelengths of 635 versus 670 nm at an excitation wavelength of 442 nm for IL2-deficient upper colon with mild colitis and healthy IL2-deficient colon. The IL2-deficient mild colitis and healthy colon emission intensities at 635 and 670 nm emission wavelengths overlap minimally, indicating that these two wavelengths can be used to categorize the two groups diagnostically.

between the IL2-deficient IBD colon and the IL2-deficient healthy colon in the scatter plot of 635- versus 670-nm emission intensity (Figure 9) suggests that these 2 groups may be distinguishable based on these 2 emission wavelengths. It is important to note that these data reflect only 1 sample in the IBD group and should be repeated to confirm that the results do not differ with increased numbers of IBD samples.

Surprisingly, the Apc$^{Min}$ adenoma and dysplasia spectra were not distinguishable from the nondiseased Apc$^{Min}$ and control mice spectra; these findings are contrary to those in the recent literature, which maintain that changes in collagen, NADH, and hemoglobin can be used to distinguish adenomatous from healthy colon in humans.[15] However, the pathologies of the Apc$^{Min}$ mice were early in stage, and it is possible that the biochemical changes that had taken place were too undeveloped to be detected by LIF. In addition, the numbers of animals and lesions included in the analysis were small and may further explain the lack of significant difference. In this study, the adenomas and dysplasias were grouped together when compared with other classifications because these 2 disease types lacked appreciable differences in fluorescence spectra and are similar in pathology.

The Peyer patches observed in the small intestine and colon were spectrally indistinguishable from healthy colonic tissue in the same respective regions of the GI tract from both normal and diseased mouse groups, therefore LIF appears to classify Peyer patches and intestinal mucosa similarly. Because Peyer patches can be difficult to differentiate from IBD by using OCT only, LIF may be important for correct classification. This example supports the benefit of combining these 2 modalities.

Of the original 150 tissue samples imaged with OCT-LIF, 46 were removed from analysis (Table 3). The largest percentage of the removed data was due to tissue preparation error, primarily partially opened lumens during longitudinal opening where the tissue was still cylindrical instead of flat during imaging (59% of data removed, 18% of total data). This problem occurred in high
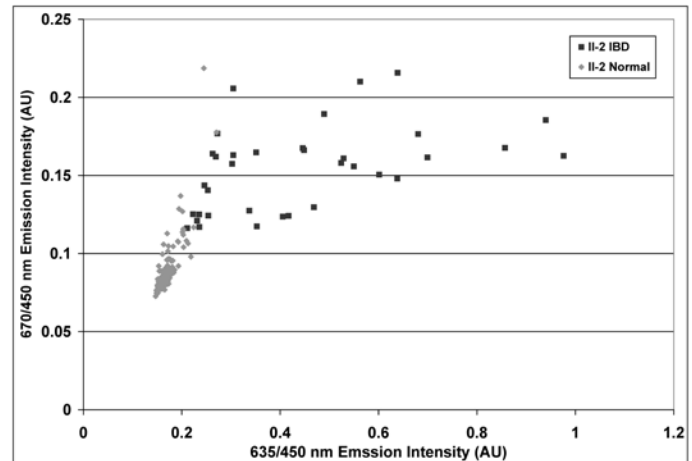
frequency with esophageal tissue samples, which has the smallest luminal diameter and is the most fragile of the tissue samples evaluated in this study. This error can largely be alleviated with improved protocols for opening the lumen. It is important to note that only 10.6% of the total data experienced either OCT or LIF technologic error. Of this error, the majority was due to LIF technologic error, primarily from incorrect background measurement or subtraction and intensity saturation. These errors may be reduced with improved protocols to improve calibration and with increased attention to saturation.

## Conclusion

We surveyed the GI tract of a variety of mouse strains and ages ex vivo as well as a model of colorectal cancer and IBD by using an OCT-LIF combined system. OCT successfully imaged samples of colon, esophagus, and small intestine, providing structural information about the tissues that correlated well with corresponding histologic sections and allowing preliminary image characteristics of healthy mouse GI to be identified. In addition, OCT identified early disease in the form of adenomas, dysplasias, and IBD and allowed the development of initial image criteria to identify and possibly distinguish these diseases from each other and from healthy tissue. LIF enabled characterization of the biochemistry of endogenous fluorophores in mouse colon, esophagus, and small intestine, providing information on collagen, NADH, and hemoglobin. Fluorescence spectra of the IBD sample exhibited peaks at 635 and 670 nm, believed to correspond to bacterial porphyrin; these peaks may have the potential to act as diagnostic markers for IBD. LIF spectra of all other tissue classifications were found to have no significant differences, including adenomas and dysplasias of the small intestine; however, we attributed this result to the early disease state and the small number of animals and pathologies.

Our preliminary data suggest that together, OCT and LIF can potentially be used to distinguish the categories of normal, Peyer patch, adenoma or dysplasia, and IBD. Therefore combined OCT-LIF may be another tool for evaluating the GI tract of mouse

models and may provide the capability to monitor the effects of drug treatment and experimental therapies in mouse models of human disease. Further studies with more diseased animals are needed to fully assess the significance of our findings. Both OCT and fluorescence spectroscopy have the capability to be used for in vivo imaging applications of the GI tract, as they are both readily adaptable to small-diameter endoscopic packaging with relative ease. Future work includes developing smaller-diameter endoscopes for endoscopic esophageal imaging and laparoscopic small intestine and upper colon imaging.

## Acknowledgments

## References

1. **Barbour KW, Davis T, White A, Baumann H, Berger FG.** 2001. Haptoglobin, inflammation, and tumorigenesis in the Min mouse. Redox Rep **6:**366–368.
2. **Barton JK, Guzman F, Tumlinson A.** 2004. Dual modality instrument for simultaneous optical coherence tomography imaging and fluorescence spectroscopy. J Biomed Opt **9:**618–623.
3. **Bouma BE, Tearney GJ, Yabushita H, Shishkov M, Kauffman CR, DeJoseph Gauthier D, MacNeill BD, Houser SL, Aretz HT, Halpern EF, Jang IK.** 2003. Evaluation of intracoronary stenting by intravascular optical coherence tomography. Heart 89:317–320.
4. **Erdman SH, Ignatenko NA, Powell MB, Blohm-Mangone KA, Holubec H, Guillen-Rodriguez JM, Gerner EW.** 1999. APC-dependent changes in expression of genes influencing polyamine metabolism, and consequences for gastrointestinal carcinogenesis, in the Min mouse. Carcinogenesis **20:**1709–1713.
5. **Gossage KW, Tkaczyk TS, Rodriguez JJ, Barton JK.** 2003. Texture analysis of optical coherence tomography images: feasibility for tissue classification. J Biomed Opt **8:**570–575.
6. **Hariri LP, Tumlinson AR, Besselsen DG, Utzinger U, Gerner EW, Barton JK.** 2006. Endoscopic optical coherence tomography and laser-induced fluorescence spectroscopy in a murine colon cancer model. Lasers Surg Med **38:**305–313.
7. **Huang D, Li Y, Radhakrishnan S.** 2004. Optical coherence tomography of the anterior segment of the eye. Ophthalmol Clin North Am **17:**1–6.
8. **Junqueira LC, Carneiro J.** 2003. Digestive tract. In: Basic histology: text and atlas, 10th ed. New York: Lange Medical Books McGraw-Hill. p 291–324.
9. **Kobayashi K, Izatt JA, Kulkarni MD, Willis J, Sivak MV Jr.** 1998. High-resolution cross-sectional imaging of the gastrointestinal tract using optical coherence tomography: preliminary results. Gastrointest Endosc **47:**515–523.
10. **Kuranov RV, Sapozhnikova VV, Shakhova HM, Gelikonov VM, Zagainova EV, Petrova SA.** 2002. Combined application of optical methods to increase the information content of optical coherent tomography in diagnostics of neoplastic processes. Quantum Electron **32:**993–998.
11. **McNally JB, Kirkpatrick ND, Hariri LP, Tumlinson AR, Besselsen DG, Gerner EW, Utzinger U, Barton JK.** 2006. Task-based imaging of colon cancer in the Apc(Min/+) mouse model. Appl Opt **45:**3049–3062.
12. **Nishioka NS, Brand S, Bouma BE, Tearney GJ, Compton CC.** 2002. Gastrointestinal applications of optical coherence tomography. In: Bouma BE, Tearney GJ, editors. Handbook of optical coherence tomography. New York: Marcel Dekker. p 673–691.
13. **Owen DA, Kelly JK.** 1994. Diseases of the large bowel. In: Atlas of gastrointestinal pathology. Philadelphia: W B Saunders Company. p 131–184.
14. **Pitris C, Jesser C, Boppart SA, Stamper D, Brezinski ME, Fujimoto JG.** 2000. Feasibility of optical coherence tomography for high-resolution imaging of human gastrointestinal tract malignancies. J Gastroenterol **35:**87–92.
15. **Prosst RL, Gahlen J.** 2002. Fluorescence diagnosis of colorectal neoplasms: a review of clinical applications. Int J Colorectal Dis **17:**1–10.
16. **Sadlack B, Merz H, Schorle H, Schimpl A, Feller AC, Horak I.** 1993. Ulcerative colitis-like disease in mice with a disrupted interleukin-2 gene. Cell **75:**253–261.
17. **Sivak Jr. MV, Kobayashi K, Izatt JA, Rollins AM, Ung-Runyawee R, Chak A, Wong RCK, Isenberg GA, Willis J.** 2000. High-resolution endoscopic imaging of the GI tract using optical coherence tomography. Gastrointest Endosc **51(4 Pt 1):**474–479.
18. **Su LK, Kinzler KW, Vogelstein B, Preisinger AC, Moser AR, Luongo C, Gould KA, Dove WF.** 1992. Multiple intestinal neoplasia caused by a mutation in the murine homolog of the *APC* gene. Science **256:**668–670.
19. **Taubinsky IM, Alexandrov MT, Koz'ma SY, Chernyi VV.** 2000. Fluorescence spectroscopy application in the express-evaluation of the gastrointestinal microflora. Crit Rev Biomed Eng **28:**145–159.
20. **Wang RK, Elder JB.** 2002. High resolution optical coherence tomographic imaging of soft biological tissues. Laser Physics **12:**611–616.